Identification of Young's Modulus from Indentation Testing and Inverse Analysis

Joris Prou, Kikuo Kishimoto, Andrei Constantinescu

JSME
Technical Journal

Vol.3, No.3, 2009

Identification of Young's Modulus from Indentation Testing and Inverse Analysis*

Joris PROU**, Kikuo KISHIMOTO*** and Andrei CONSTANTINESCU†

** Tokyo Institute of Technology, Department of Mechanical Sciences and Engineering
O-okayama, Meguro-ku, Tokyo 152, Japan
E-mail: prou.j.aa@m.titech.ac.jp

*** Tokyo Institute of Technology, Department of Mechanical Sciences and Engineering
O-okayama, Meguro-ku, Tokyo 152, Japan
E-mail: kkishimo@mep.titech.ac.jp

† École Polytechnique, Laboratoire de Mécanique des Solides (CNRS UMR 7649)
91128 Palaiseau cedex, France
E-mail: constant@lms.polytechnique.fr

Abstract

In this study, a numerical method for the identification of the Young's modulus of linear elastic coated materials from continuous indentation test is first presented. The identification is based on an inverse analysis where the minimization of a cost functional is performed by a gradient descent algorithm. The main result is the computation of cost function gradient by using a direct differentiation technique, resulting in a time-saving method compared to the widely used finite difference method. The validity and illustration of this approach is shown through several numerical examples. The second part of this article is dedicated to the identification of elasto-plastic thin films Young's modulus. A new method is proposed, where the inverse analysis relies only on finite element computations for elastic materials.

Key words : indentation, thin films, Direct Differentiation Method, inverse analysis

1. Introduction

The indentation test has been first introduced for quality control on materials, using the concept of hardness proposed by Brinell[1),(2)] as the ratio between the applied forces and effective contact surface. The technological progress has made possible the improvement of this test apparatus and now the force and displacement of the indenter can continously and simultaneously be recorded. The precision of the displacement measurement can actually reach the sub-nanometer scale. The fact that indentation can be performed directly on the surface of the material without a specimen machining, imposed the indentation test along the atomic force microscopy as the leading mechanical test device for a large range of applications including microelectronics, thin films, coatings, etc.

In spite of the apparent simplicity of the test, the nonlinearity of the contact condition will induce complex mechanical strain and stress fields even in the case of a linear material behavior. Elastic solutions are based essentially on the fondamental Green functions stemming from the rigid indenter solution proposed by Boussinesq in 1885 for a bulk material, integral transforms as developped in the pioneering work of Sneddon[3)], etc., as presented in the monographs[1),(4)]. In the case of thin films, elastic solutions are based on the same mathematical methods.

The techniques used for the elastic materials are of limited interest in the case of nonlinear material behaviour like plasticity or viscoelasticity. The closed-form solutions are based on plastic flow rules as proposed in the pioneering work of Prandtl[5)] and the elastic solution has been only used to deduce the Young's modulus from the unloading part of the load-

*Received 21 Dec., 2009 (No. XX-XXXX)
[DOI: 10.1299/jmmp.3.1]

displacement curve, which can be resumed as the Oliver-Pharr[6] and the Doerner-Nix[7] methods. They are generally integrated in the indentation apparatus. These two methods assume that the beginning of the unloading is elastic. They make use of the following semi-empirical relation first established by Loubet *et al.*[8]:

$$E^* = \frac{1}{2}\sqrt{\frac{\pi}{A_c}}S \tag{1}$$

where S denotes the initial slope at the initial state of the unload, A_c the projected contact area at maximum load and E^* the effective modulus defined by $\frac{1}{E*} = \frac{1-\nu^2}{E} + \frac{1-\nu_{ind}^2}{E_{ind}}$ in order to take into account the non-perfect rigidity of the indenter (where the subscript *ind* stands for indenter).

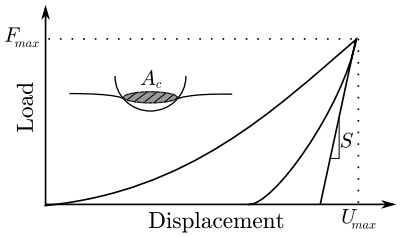

Fig. 1 Typical load displacement curve of the indenter

The difficulties with the direct use of this relation come from the inaccurate evaluation of the contact surface, as when pile-up or sink-in effect at contact surface becomes important (Fig. 2), or from the existence of a thin film which changes the apparent contact modulus at the surface.

The above two methods propose different respective method to evaluate A_c, leading to efficient and practical way to evaluate bulk materials Young's modulus, and in most cases an estimation with less than 10% error can be achieved[9].

For coated materials, in order to avoid the substrate influence on the load displacement curve, a general practical rule is to consider that, for an indentation with a maximum penetration of 10% of the coating thickness, the above methods can still be applied. Though, it was pointed out in case of superhard coatings in[10),(11)] that this rule is insufficient to obtain precise results. Moreover, it should be noted that, for very thin films (few dozens of nanometers) performing an indentation at 10% of the thickness is limited by the precision of the apparatus, and indenter size problems. The projected contact area is calculated amongst others by the assumed geometry of the indenter, however for sharp indenters, indenter tips are not perfect and show roundness with a finite radius tip of 50 nm or more. Thus, when shallow indentation is performed for the same order indentation depth, the contact occurs at the rounded part of the tip leading to errors in Young's modulus estimations.

Introduction of correction factors to improve the accuracy of those methods in case of piling-up or substrate effect have been proposed, and more details can be found in[2].

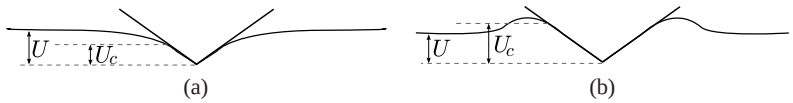

Fig. 2 Contact depth U_c related to: (a) sink-in - (b) pile-up

A complementary approach to the direct identification formulae, is to try to extract the information about the mechanical properties directly from the load-displacement indentation curves, by making use of inverse analysis. Within the wide literature in this domain we can mention e.g. for bulk material[12),(13)], for thin films[14].

Inverse analyses are generally based on the minimization of a cost function measuring the discrepancy between experimental load-displacement curve and a simulated one. The

minimization is then done numerically using gradient based or exploratory algorithms. It is equally important to notice that for this problem we do not actually dispose of a formal proof of the uniqueness or stability of the solution with respect to input data. Although some researchers made successful attempts to use exploratory algorithms in certain particular cases e.g. in[14], these methods require a large number of estimations of the direct problem and this leads to important computational time, due to the complexity of the inverse problem.

The faster option is the identification using gradient-based algorithms. Most of the studies found in literature[12] are based on the estimation of the gradient using the finite difference method, which is straightforward to implement but can be as well time-consuming as the number of paramaters to identify becomes important.

The gradient can also be obtained using the adjoint method[15] or the direct differentiation technique. If the adjoint state method permits a direct computation of the gradient for a large number of parameters using only one additional computation, it presents a major inconveniance when applied to nonlinear problems that new adjoint constitutive laws have to be implemented in order to perform the optimization.

The advantage of the direct differentation technique is its formal simplicity, as well as the possibility to extend easily to nonlinear problems, both in terms of material constitutive nonlinearity as in terms of geometric nonlinearity (large displacement and rotations).

The present work presents the computation of the gradient using the direct differentiation method in the case of a elastic indentation problem and its application to evaluate the Young's modulus of thin films materials both in the case of elastic and elastoplastic materials. The restriction to elastic problems is done only for the sake of clarity in the presentation of the direct differentiation method and does not restrict the generality of the technique. The next section recalls the direct problem both in the continuous and finite element formulations. This part is followed by details of the finite element model and a brief description of the inverse analysis. The fourth section describes in detail the direct differentiation method, and its accuracy is illustrated by comparison with closed-form solution derived from Sneddon[3]. Finally, numerical examples for the identification of Young's modulus in the case of thin films are given. In the first series of examples the materials are elastic and the identification is done from the loading curve. In the second series of examples the materials are elastoplastic and the identification is done on the unloading curve using a similar strategy as presented in the closed-form solution of Doerner-Nix, Oliver-Pharr or as presented in the work of Vlassak et al.[16] based on the analytical solution of the contact problem of axisymmetric indenter on a layered elastic half-space.

2. Direct Problem

2.1. Continuous Formulation

The elastic material is defined by its domain Ω of boundary Γ. This boundary can be divided in three parts Γ_u, Γ_t and Γ_c forming a partition of Γ. Γ_u, Γ_t and Γ_c are respectively the surface of imposed displacement, the surface of imposed tractions and the surface where the contact may occur.

$$\Gamma = \Gamma_t \cup \Gamma_u \cup \Gamma_c\,, \qquad \Gamma_t \cap \Gamma_u = \Gamma_t \cap \Gamma_c = \Gamma_c \cap \Gamma_u = \emptyset \tag{2}$$

The surface where contact effectively occurs is denoted by Γ_c^{eff}.

The indenter is considered as a rigid body and its imposed displacement is noted U_k. The above notations can be visualized from Fig. 3. Since there are no volumetric forces acting on the material, the balance equation can be written as:

$$div\,\boldsymbol{\sigma} = \mathbf{0} \qquad \text{in } \Omega \tag{3}$$

The relation between displacement and strains under the assumption of small strains is defined as:

$$\boldsymbol{\varepsilon}(\boldsymbol{u}) = \frac{1}{2}\left(\boldsymbol{\nabla u} + \boldsymbol{\nabla}^T \boldsymbol{u}\right) \qquad \text{in } \Omega \tag{4}$$

For linear elastic materials, the constitutive equation is given by:

$$\boldsymbol{\sigma}(\boldsymbol{u}) = \boldsymbol{C}(\boldsymbol{c}) : \boldsymbol{\varepsilon}(\boldsymbol{u}) \qquad \text{in } \Omega \tag{5}$$

where $\boldsymbol{C}$ is the fourth-order tensor of the elastic moduli and $\boldsymbol{c}$ is the tensor of material parmeters characterizing the spatial distribution (thickness of layers, for example) and moduli. We recall that for isotropic materials, it is expressed as:

$$\boldsymbol{C} = 3\lambda\boldsymbol{\mathcal{I}} + 2G\boldsymbol{\mathcal{J}} \tag{6}$$

with λ and G are the two Lamé parameters defined as $\lambda = \frac{\nu E}{(1+\nu)(1-2\nu)}$ and $G = \frac{E}{2(1-\nu)}$, in terms of the Young's modulus E and Poisson's ratio ν. $\boldsymbol{\mathcal{I}}$ and $\boldsymbol{\mathcal{J}}$ denote respectively the fourth-order identity tensor (for second-order tensor) and the fourth-order tensor defining the projection on the volumetric tensor subspace.

Boundary conditions

Two types of different boundary conditions can be imposed on Γ: displacements corresponding to Dirichlet boundary conditions on Γ_u, and forces corresponding to Neumann type boundary conditions, on $\Gamma_t \cup \Gamma_c$. The corresponding boundary conditions are:

$$\begin{cases} \boldsymbol{u} = \boldsymbol{u}^d = \boldsymbol{0} & \text{on } \Gamma_u \\ \boldsymbol{\sigma} \cdot \boldsymbol{n} = \boldsymbol{t}^n = \boldsymbol{0} & \text{on } \Gamma_t \end{cases} \tag{7}$$

For the contact surface Γ_c, the boundary conditions can be expressed by the Signorini contact conditions. With the following notations, $u_n = \boldsymbol{u} \cdot \boldsymbol{n}$, $\sigma_n(\boldsymbol{u}) = \boldsymbol{\sigma}(\boldsymbol{u}) \cdot \boldsymbol{n} \cdot \boldsymbol{n}$ ($\boldsymbol{n}$ is the normal unit vector to the surface), The signorini conditions are defined as:

$$\begin{cases} u_n - g - U_k \leq 0 \\ \sigma_n(\boldsymbol{u}) \leq 0 \\ (u_n - g - U)\,\sigma_n(\boldsymbol{u}) = 0 \end{cases} \qquad \text{on } \Gamma_c \tag{8}$$

where $g \geq 0$ is the gap function, distance between the indenter and indented material before the indentation. It represents then the shape of the indenter.

The first equation is the unilateral contact condition expressing the physical impossibility for the indenter to penetrate into the surface of the indented material. The second one is the mathematical traduction that the stress must be compressive. The last one implies that for the points on the surface of the material, which are not in contact with the indenter $u_n - g - U_k < 0$ there is no stress transmission.

From the above formulations, the effective contact area is not known in advance, leading to nonlinearity even for elastic materials, and then require the use of incremental method in the finite element code. The imposed displacement on the indenter is then applied by increments, such as $U_{i+1} = U_i + \Delta U_i$

The computation of the gradient requires to estimate the evolution of the contact area with respect to material parameters. It has been proven[15] that the variation can be neglected at the first order. Therefore the differentiated problem is defined on the effective contact area Γ_c^{eff}. The differentiated problem is equivalent to an elastic problem for the indented material with imposed displacement on the contact surface.

The differentiated equivalent problem at the step k, corresponding to a displacement U_k of the indenter (Fig. 4), is given by the following boundary conditions:

$$\begin{cases} \boldsymbol{\sigma} \cdot \boldsymbol{n} = \boldsymbol{t}^n = \boldsymbol{0} & \text{on } \Gamma_t \\ \boldsymbol{u} = \boldsymbol{u}^d = \boldsymbol{0} & \text{on } \Gamma_u^1 \\ \boldsymbol{u} = \boldsymbol{u}^d = \boldsymbol{U}_k & \text{on } \Gamma_u^2 = \Gamma_c^{eff} \end{cases} \qquad \text{where } \Gamma_u = \Gamma_u^1 \cup \Gamma_u^2 \tag{9}$$

The validity of this statement is verified a posteriori by comparing the sensitivities obtained by the direct differentiation method with the one provided by Sneddon analytical solution for infinite elastic half-space as described in §4.2.

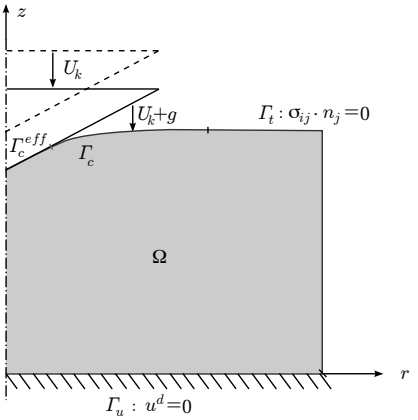

Fig. 3 Scheme of the direct problem

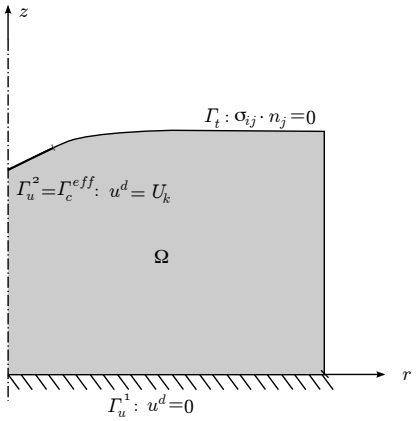

Fig. 4 Scheme of the equivalent problem

2.2. Finite Element Implementation

This section describes the implementation in the finite element program of problem dealing with imposed displacement conditions.

The potential energy for an elastic body defined by the previously described equivalent problem is given by:

$$W(\boldsymbol{v}) = \int_\Omega \boldsymbol{\varepsilon}(\boldsymbol{v}) : \boldsymbol{C} : \boldsymbol{\varepsilon}(\boldsymbol{v}) d\Omega + \int_{\Gamma_t} \boldsymbol{t^n} \cdot \boldsymbol{v} d\Gamma \tag{10}$$

where in the considered case $\boldsymbol{t^n} = \boldsymbol{0}$ and $\boldsymbol{v}$ should satisfy the imposed displacement boundary conditions $\boldsymbol{v} \in \mathcal{U}$

$$\begin{aligned} \mathcal{U} &= \left\{ \boldsymbol{u} \in H^1(\Omega) \,|\, \boldsymbol{u} = \boldsymbol{0} \text{ on } \Gamma_u^1 \text{ and } \boldsymbol{u} = \boldsymbol{U}_k \text{ on } \Gamma_u^2 \right\} \\ \mathcal{U} &= \left\{ \boldsymbol{u} \in H^1(\Omega) \,|\, \boldsymbol{u} = \boldsymbol{u^d} \text{ on } \Gamma_u \right\} \end{aligned} \tag{11}$$

The displacement field solution of the elastic problem is the minimizer of the potential energy. In order to solve this constrained minimization problem, it is natural to introduce the Lagrangian $\mathcal{L}$ associated to the constraint of the imposed displacement, where now $\boldsymbol{v}$ is a vector of $H^1(\Omega)$.

$$\mathcal{L}(\boldsymbol{v}) = \int_\Omega \boldsymbol{\varepsilon}(\boldsymbol{v}) : \boldsymbol{C} : \boldsymbol{\varepsilon}(\boldsymbol{v}) d\Omega + \int_{\Gamma_t} \boldsymbol{t}^n \cdot \boldsymbol{v} d\Gamma + \int_{\Gamma_u} \boldsymbol{\lambda} \cdot (\boldsymbol{v} - \boldsymbol{u^d}) d\Gamma \tag{12}$$

where $\boldsymbol{\lambda}$ is the Lagrange multiplier vector related to the constraint of the imposed displacement and correspond to the physical reaction forces this imposed displacement induces.

With the finite element notations, the Lagrangian can be written as:

$$\mathcal{L}(\boldsymbol{V}) = \boldsymbol{V}^T \boldsymbol{K} \boldsymbol{V} + \boldsymbol{F}^T \boldsymbol{V} + \boldsymbol{\lambda}^T \left(\boldsymbol{P} \boldsymbol{V} - \boldsymbol{U^d} \right) \tag{13}$$

where $\boldsymbol{V}$ is the nodal displacement vector, $\boldsymbol{K}$ the stiffness matrix. Furthermore $\boldsymbol{K}$ defined as:

$$\boldsymbol{K} = \int_\Omega \boldsymbol{B} \boldsymbol{C} \boldsymbol{B} d\Omega \tag{14}$$

with $\boldsymbol{B}$ the matrix of first order derivative operator, $\boldsymbol{Bu}$ corresponding thus to the strain vector.

$\boldsymbol{F}$ is the imposed load vector defined by:

$$\boldsymbol{F} = \int_{\Gamma_t} \boldsymbol{t}^n d\Omega \tag{15}$$

$\boldsymbol{\lambda}$ is the Lagrange multiplier vector related to the imposed displacement constraint (reaction forces) and $\boldsymbol{P}$ is the projection matrix on the nodes of imposed displacement conditions:

$$\boldsymbol{P} : \boldsymbol{U} \longmapsto \boldsymbol{U}_{|\Gamma_u} \tag{16}$$

The constrained minimization of the potential energy with respect to $\boldsymbol{v}$ satisfying the imposed displacement boundary conditions, is equivalent with finding the saddle point of the Lagrangian for any $\boldsymbol{v} \in H^1(\Omega)$.

The stationarity conditions for the Lagrangian are expressed as follows:

$$\begin{cases} \dfrac{\partial \mathcal{L}}{\partial \boldsymbol{V}}(\boldsymbol{U}) = 0 = \boldsymbol{K}\boldsymbol{U} + \boldsymbol{P}^T\boldsymbol{\lambda} - \boldsymbol{F} \\ \dfrac{\partial \mathcal{L}}{\partial \boldsymbol{\lambda}}(\boldsymbol{U}) = 0 = \boldsymbol{P}\boldsymbol{U} - \boldsymbol{U}^d \end{cases} \tag{17}$$

which rearranged in a matrix form, gives:

$$\begin{bmatrix} \boldsymbol{K} & \boldsymbol{P}^T \\ \boldsymbol{P} & 0 \end{bmatrix} \begin{bmatrix} \boldsymbol{U} \\ \boldsymbol{\lambda} \end{bmatrix} = \begin{bmatrix} \boldsymbol{F} \\ \boldsymbol{U}^d \end{bmatrix} \tag{18}$$

The above linear system corresponds to the finite element formulation of an elastic problem with imposed displacement conditions.

3. Inverse Problem

The identification of model parameters can be seen as an inverse problem that can be summed summarized in this case as: *identifying the mechanical parameters of the material constitutive law from the knowledge of the indentation load-displacement curve*. This section describes the choice made for the direct problem and presents the inverse analysis.

3.1. Finite Element Model of the Direct Problem

The direct problem model is computed here by finite element simulation, with the open-source finite element software CASTEM[17]. So that the computation time is decreased and thanks to the symmetry of the problem, an axisymmetric model is employed. We made the following choices: films and substrate are considered to be perfectly bonded, imposed displacement conditions on the indenter are used, and the indenter is assumed to be rigid.

The mesh used in the simulation was created with a refinement near the indentation zone where the stress is maximum, and the contact surface was refined to ensure its precise computation (Fig. 5).

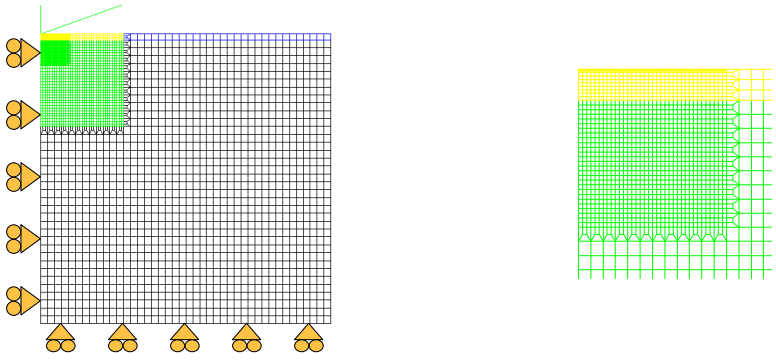

Fig. 5 Mesh of the finite element simulation with zoom around the indentation zone

3.2. Inverse Analysis Scheme

The description of the direct problem model permits to compute a load-displacement curve for a given set of mechanical parameters, by finite element computation. The inverse analysis is based on the minimization of a cost functional measuring the discrepancy between the measured data and the one computed from the direct problem model. Its expression for the indentation test can be expressed as in Eq. (19).

$$J = \frac{1}{2}\sum_{k=1}^{n}\left(F_{comp}(U_k) - F_{meas}(U_k)\right)^2 \tag{19}$$

F_{meas} and F_{comp} are respectively the reaction force on the indenter obtained from measurement and computation of the direct problem. U_k is the displacement of the indenter at a chosen increment k.

Several approaches can be considered for the minimization of the cost functional. Exploratory algorithms such as simplex method or genetic algorithms are only based on the evaluation of the cost functional. These algorithms provide the global minimum, but require a large number of computations of the direct problem. Estimating that non-uniqueness is not the main issue in this context, a gradient based algorithm (Levenberg-Marquardt) is used here. This type of algorithm using the information of the derivative of the cost functional is faster than the exploratory algorithms, but if the initial guess is too far from the solution, they can be trapped in a local minimum. This choice of algorithm implies to decide for a gradient computation. Three techniques are possible:

- the finite difference method
- the direct differentiation method
- the adjoint state method

A detailed description of these technique in the case of linear problems can be found in[18]. Let us mention that the finite difference method is costly as multiple computations of the finite element problem are required to compute the gradient and that the precision is dependent of several numerical factors which are difficult to control.

Moreover, in our case where contact boundary conditions are involved, the problem is nonlinear even for a linear material behaviour and several difficulties will occur in this case. A general discussion of the differentiation of the contact problem has been already presented in[15], where the adjoint state method has been proposed as a technique to solve compute the gradient.

Next we shall explore the application of the *direct differentiation method* in the case of contact boundary conditions. This is justified as this method can then easily be extended to nonlinear material behaviour, which is not the case of the adjoint state method. In the later case, one has to completely recompute the constitutive law (see[15]).

4. The Sensitivity Problem

4.1. Elasticity and Stiffness Matrix

This section presents the application of the direct differentiation method to the elastic problem for the evaluation of the cost function gradient.

From the definition of the cost function in Eq. (19), one can remark that the i^{th} component of the gradient, corresponding to the parameter c_i, is given by:

$$\frac{\partial \mathcal{J}}{\partial c_i}(\boldsymbol{c}) = \frac{1}{2}\sum_{k=1}^{n}(F^k_{comp}(\boldsymbol{c}) - F^k_{meas})\frac{\partial F^k_{comp}}{\partial c_i}(\boldsymbol{c}) \tag{20}$$

where the upper-script k refers to the displacement indenter $U = U^k$.

As the first term on the right-hand side is known from the experimental and computed data, the only remaining term to be computed is $\frac{\partial F^k_{comp}}{\partial c_i}$, which is the sensitivity (partial derivative) of the computed reaction force on the indenter with respect the parameter c_i.

The following notation is introduced for the sensitivity with respect to c_i : $\frac{\partial}{\partial c_i} \equiv \delta_{c_i}$

By taking the partial derivative of the linear system in Eq. (18) with respect to c_i and since the imposed displacement and tractions do not depend on the parameter c_i:

$$\begin{bmatrix} \boldsymbol{K} & \boldsymbol{P}^T \\ \boldsymbol{P} & 0 \end{bmatrix}\begin{bmatrix} \delta_{c_i}\boldsymbol{U} \\ \delta_{c_i}\boldsymbol{\lambda} \end{bmatrix} = -\begin{bmatrix} \delta_{c_i}\boldsymbol{K} & 0 \\ 0 & 0 \end{bmatrix}\begin{bmatrix} \boldsymbol{U} \\ \boldsymbol{\lambda} \end{bmatrix} = -\begin{bmatrix} \delta_{c_i}\boldsymbol{K}\boldsymbol{U} \\ 0 \end{bmatrix} \tag{21}$$

In order to solve the above linear system, the sensitivity of the stiffness matrix K needs to be computed. From Eq.(14), it follows that:

$$\delta_{c_i}\boldsymbol{K} = \int_\Omega \boldsymbol{B}\delta_{c_i}\boldsymbol{C}\boldsymbol{B}d\Omega \tag{22}$$

The sensitivity of the elastic moduli operator $\delta_{c_i}\boldsymbol{C}$, is obtained from the definition of $\boldsymbol{C}$ in Eq. (6), such as:

$$\delta_{c_i}\boldsymbol{C} = 3\delta_{c_i}\lambda\boldsymbol{\mathcal{I}} + 2\delta_{c_i}G\boldsymbol{\mathcal{J}} \tag{23}$$

4.2. Validation of the Equivalent Problem for Contact Conditions

The sensitivity computation relative to contact conditions has been discussed in details in several works for contacts involving friction or not[19), (20)].

The objective next is to validate the proposition that the contact area does not change for a small variation in the parameters. The validation will be done by numerical experiment and comparing the numerical computation with the closed-form solution for an elastic half-space proposed by Sneddon.

Under the assumption of a rigid indenter, the Sneddon relation is:

$$F = \frac{2}{\pi}\tan(\theta)\frac{E}{1-\nu^2}U^2 \tag{24}$$

From the above, the sensitivity of F with respect to the Young's modulus is given by:

$$\frac{\partial F}{\partial E} = \frac{2}{\pi}\tan(\theta)\frac{1}{1-\nu^2}U^2 \tag{25}$$

The bulk material used for this simulation is a common steel with Young's modulus E = 205 GPa and Poisson's ratio $\nu = 0.3$. The dimensions of the specimen were $100 \times 100\ \mu$m and as the indented material should behave as an infinite half space, the maximum penetration of the indenter $U_{max} = 1.5\ \mu$m was chosen.

The sensitivities with respect to the Young's modulus obtained from finite difference, direct differentiation and the Sneddon relation are investigated here. The application of the direct differentiation method requires the sensitivity of the elastic moduli operator $\delta_{c_i}\boldsymbol{C}$ (Eq. (23)). For the simple case of a bulk material, it follows that:

$$\delta_{c_i}\boldsymbol{C} = 3\frac{1}{E}\lambda\boldsymbol{\mathcal{I}} + 2\frac{1}{E}G\boldsymbol{\mathcal{J}} \tag{26}$$

For the finite difference method, the center difference was employed with the discretization step $\Delta E = E/1000$, as smaller discretization steps gave the same results.

The comparison of the sensitivities obtained by the different methods is presented in Fig. 6. It ensures the validity of the method and the equivalent problem hypothesis. As mentioned in §3.2, the direct differentiation can give more accurate results than the finite differences. Moreover, to obtain the load-displacement curve and compute the sensitivity of

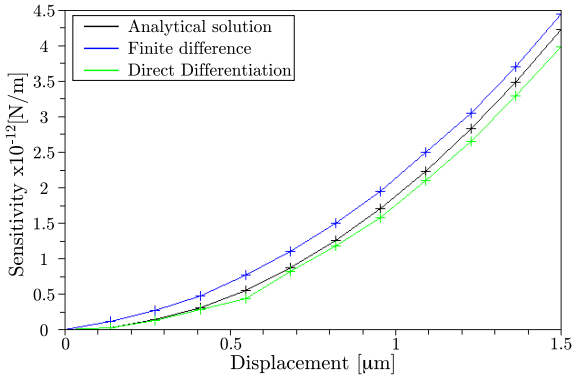

Fig. 6 Comparison of the sensitivities from finite difference and direct differentiation

the Young's modulus, the finite difference requires three computation of the direct problem by finite element, each one lasting T_{comp}, whereas with the direct differentiation implemented in the finite element code both of these informations were obtained in a time nearly equal to $1.2 \times T_{comp}$.

The time efficiency is more encouraging for problems with higher number of parameters. In the following, identification for the elastic case where two parameters are to be identified, the direct differentiation time was less than $1.4 \times T_{comp}$, which should be compared to $5 \times T_{comp}$ for the finite difference.

5. Identification of Elastic Films Young's modulus

5.1. Single Layer Coated Elastic Half Space

In this example, the total thickness of the indented material is $h_1 + h_2 = 100\ \mu$m, with a film thickness of $h_1 = 2\ \mu$m, the radius of the indented cylindrical specimen is 100 μm. The Poissons ratios for both film and substrate are set to $\nu = 0.3$. The identification is performed for the Young's modulus of the film noted E_1 and the Young's modulus of the substrate E_2.

The values to be identified are $E_1 = E_2 = 205$ GPa. The load-displacement curve corresponding to the experimental data is generated by finite element simulation. The maximum indentation displacement has been chosen as $U_{max} = 1.5\ \mu$m, and the gradient is computed by direct differentiation every ten steps. This value was determined relatively to a sensitivity study of the reaction force on the indenter with respect of the Young's moduli E_1 and E_2 around the solution values (Fig.7 (b)), so to have both effects of E_1 and E_2. This indicates that for shallow indentation the effect of the film is predominant, and as the indentation gets deeper the influence of the substrate increases and exceeds the substrate one when reaching $U \approx 0.45$ of the film thickness. Fig.7 (a), (c), (d) sensibility curves for different ratios E_1/E_2 around the solution, show a similar evolution of the sensibility and highlight as could be expected that the harder the film is, so is the effect of the substrate on the reaction force.

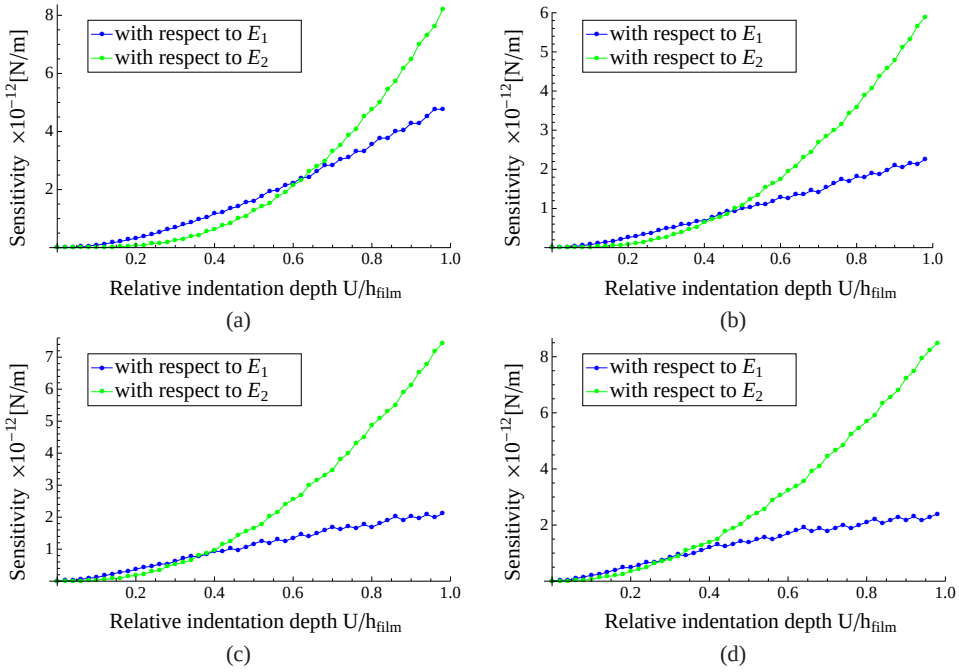

Fig. 7 Reaction force sensitivity with respect to E_1 and E_2 for: (a) $E_1/E_2 = 0.5$, (a) $E_1/E_2 = 1$, (c) $E_1/E_2 = 2$, (d) $E_1/E_2 = 4$

Gradient type minimization methods being influenced by the choice of the initial values, identification with several different initial guesses were carried out. Two of these values are presented in Table 1, and the identified ones in Table 2. The identified values were obtained with less than 0.05% error and in both cases in less than 15 iterations.

Table 1 Test conditions

	E_1 [MPa]	E_2 [MPa]
Solution	205000	205000
Init. guess 1	400000	400000
Init. guess 2	400000	100000

Table 2 Identified parameters

Init. guess	E_1 [MPa]	rel. error	E_2 [MPa]	Rel. error
1	204907	0.0454	205002	0.000976
2	205003	0.00146	204999	0.000488

An illustration of this results is displayed in Figs. 8 and 9. Figure 8 is a representation of the cost function for values of E_1 and E_2 taken between 50 and 500 GPa. This curve was obtained by interpolation between 49 values regularly spaced in $[50, 500] \times [50, 500]$ by a

polynomial function. As there is only a global minimum and no flat valley, the identification was easily performed. The identification paths in Fig. 9 show the influence of the initial guess and the gradient slope at this point on the number of iteration required for the identification.

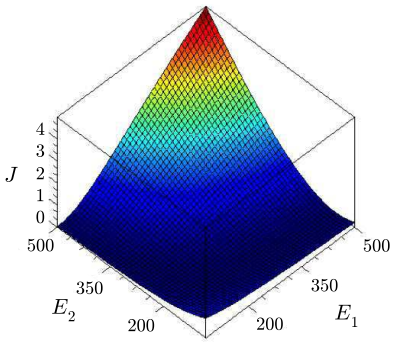

Fig. 8 Topology of the cost functional

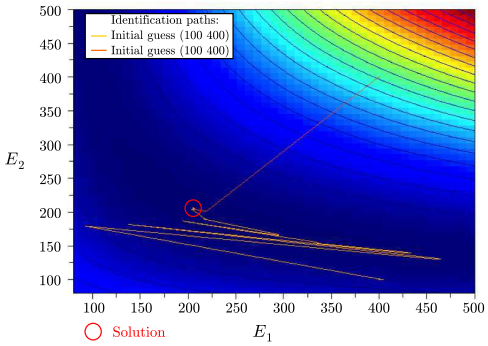

Fig. 9 Cost functional with identification paths

5.2. Bi-Layer Coated Elastic Half Space

In this second example, the indented material is composed of two layers deposited on a substrate. The thickness of the whole material is $h_1 + h_2 + h_3 = 5000\ \mu$m. The thicknesses of the two layers and the substrate are noted respectively h_1, h_2 and h_3. h_1 and h_2 are not known, but the total thickness $h_1 + h_2 = 100\mu$m. E_1, E_2 and E_3 are respectively the Young's moduli of the two films and the substrate, see Fig. (10). The value of the Poisson's ratio is taken as $\nu = 0.3$. The identification is performed for the parameters h_1 and E_2.

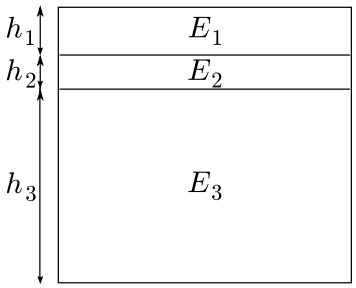

Fig. 10 Scheme for the two layers problem

The Young modulus of the substrate is supposed to be known. As the thickness of the film is 100 μm, by performing a very small indentation compared to this thickness the Young modulus at the surface can be measured, and thus is also assumed to be known. The two parameters to identify are the thickness of the upper layer h_1 and the Young modulus of the second layer.

The discontinuity of the Young's modulus at the interface between the two films lead to a singularity when computing the sensitivity with respect to h_1 of the stiffness matrix with the direct differentiation method. To overcome this difficulty, the indented layers and substrate system is considered as an unique material with a Young's modulus distribution varying with the depth. The distribution is given by the sum of two logistic functions:

$$E(z) = E_3 + (E_1 - E_2)\frac{1 + e^{-kh_1}}{1 + e^{k(z-h_1)}} + (E_2 - E_3)\frac{1 + e^{-kh_2}}{1 + e^{k(z-h_2)}} \qquad (27)$$

k is a factor that affects the variation rate, the bigger k is the closer from a step function the curve is. Here $k = 2$ is chosen. A representation of this distribution is plotted in fig. 11.

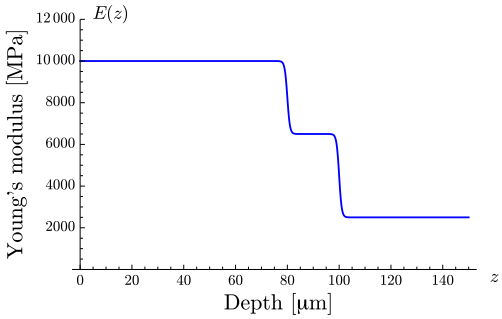

Fig. 11 Young's modulus distribution realized by logistic function

The derivatives of the elastic moduli tensor required for the direct differentiation are detailed below.

(i) For E_2

$$\frac{\partial E}{\partial E_2}(z) = \frac{1 + e^{-}kh_2}{1 + e^{k(z-h_2)}} - \frac{1 + e^{-kh_1}}{1 + e^{k(z-h_1)}} \tag{28}$$

with the above relation and the eq. (6):

$$\frac{\partial \boldsymbol{C}}{\partial E_2} = 3\frac{\partial E}{\partial E_2}\frac{\nu}{(1+\nu)(1-2\nu)}\boldsymbol{\mathcal{I}} + 2\frac{\partial E}{\partial E_2}\frac{1}{2(1-\nu)}\boldsymbol{\mathcal{J}} \tag{29}$$

(ii) For h_1

$$\frac{\partial E}{\partial h_1}(z) = (E_1 - E_2)\frac{ke^{-kh_1}(e^{kz}-1)}{(1+e^{k(z-h_1)})^2} \tag{30}$$

and then

$$\frac{\partial \boldsymbol{C}}{\partial h_1} = 3\frac{\partial E}{\partial h_1}\frac{\nu}{(1+\nu)(1-2\nu)}\boldsymbol{\mathcal{I}} + 2\frac{\partial E}{\partial h_1}\frac{1}{2(1-\nu)}\boldsymbol{\mathcal{J}} \tag{31}$$

As in the one layer case, the experimental data was simulated by finite element, and the identification performed with two different initial guesses. The corresponding values are listed in the Table 3 and the identified values in Table 4. The results are slightly different depending of the initial guess, but the identification less than 2.2% error.

Table 3 Mechanical parameters

	E_2 [MPa]	h_1 [μm]
Solution	6250	80
Init. guess 1	5000	50
Init. guess 2	10000	10

Table 4 Identified parameters

Init. guess	E_2 [MPa]	rel. error	h_1 [μm]	Rel. error
1	6386	2.18	79.168	1.04
2	6251	0.016	79.996	0.005

The evolution of the sensitivity of the reaction force with respect to the parameters E_2 and h_1 as a function of the indentation depth normalized by the film thickness is given in Fig.12. The sensitivity is plotted at the solution values of E_2 and h_1. The sensibility curves show that the effect of the thickness h_1 is greater than the one of E_2 at every indentation depth. This complies with intuition, as one can expect that a change of a few percents in h_1 would have a bigger effect on the material stiffness around the indentation zone than the same relative change of E_2. This also suggest an explanation of the better accuracy in the identification of h_1 compared to the one of E_2.

6. Identification of Elasto-Plastic Films Young's modulus

Usual inverse analyses are based on the minimization of a cost functional measuring the discrepancy between the measured data and a computed load-displacement curve obtained from finite element simulation. This requires to use plastic behavior models for the materials in the simulation in order to fit experimental data. So that even interested in the Young's

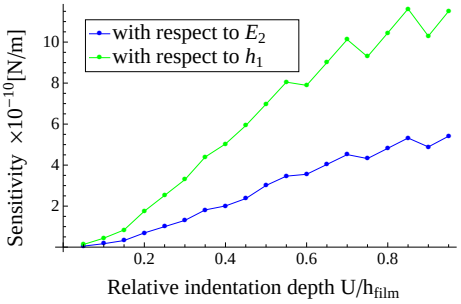

Fig. 12 Reaction force sensitivity with respect to E_2 and h_1

modulus, not only elastic properties but also all the plastic properties need to be identified, leading to heavy computations.

Here we propose a time-saving method for the identification of thin films Young's modulus, since the inverse analysis relies only on finite element computations for elastic behavior materials.

6.1. Methodology

The method proposed next is essentially based on similar concepts as Oliver-Pharr[9], Doerner-Nix[7] and also with Vlassak[16]. An important point is that the initial slope of the unloading curve for a plastic material should be equal to the tangent at the load-displacement curve for an elastic material with the same Young's modulus, if the corresponding contact area are the same (Fig. 13). Based on this a numerical procedure is proposed, which has the advantages to directly account for the substrate effect, and not to make assumptions concerning the possible pile-up or sink-in effect.

We thus propose to perform n indentations on a sample for different maximum indentation depths (subsequently different contact areas at maximum load) and to use the cost-function $\mathcal{J}$ defined in Eq. (32).

$$\mathcal{J}(E_1) = \frac{1}{2}\sum_{k=1}^{n}\left(\frac{\partial F_{comp}}{\partial U}(A^k_{cont}) - S^k_{meas}\right)^2 \tag{32}$$

where E_1 is the film Young's Modulus, $\partial F_{comp}/\partial U$ is the tangent at the computed elastic load displacement curve, A^k_{cont} is the contact area at maximum load for the k^{th} plastic indentation experiment, and S^k_{meas} the corresponding initial slope of the unloading curve.

Elastic computations only being required, the gradient of this cost function can be obtained by the previously described direct differentiation method, and except for the cost functional the inverse analysis remains the same.

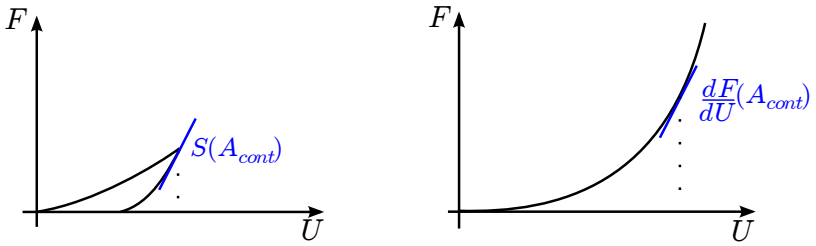

(a) (b)

Fig. 13 Correspondance of the initial unloading slope of the plastic curve (a) and the tangent to the elastic curve (b)

6.2. Numerical examples

The illustration and validation of this method is shown on several numerical examples representing indentation on perfectly plastic film and substrate, where the thickness of the

film h_1=150 μm and the one of the whole material is h_1+h_2=5000 μm. Test data correspond to three simulated indentations on elasto-plastic material, for the following maximum indentation depths: 10 μm, 20 μm, 30 μm.

Ten different sets of film and substrate were investigated numerically, whose mechanical properties are summarized in Table 5. Material sets 1 to 5 corresponding to a ratio of $1/50$ for E/σ^Y and for different ratios E_1/E_2 ranging from $1/4$ to 4, while for materials set 6 to 10 a ratio $1/500$ ratio for E/σ^Y was chosen, as a more important pile-up effect is expected.

Table 5 Mechanical properties

Material set	$E_1[GPa]$	$\sigma_1^Y[MPa]$	$E_2[GPa]$	$\sigma_2^Y[MPa]$
1	3	60	12	240
2	5	100	10	200
3	7.5	150	7.5	150
4	10	200	5	100
5	12	240	3	60
6	72	144	288	576
7	120	240	240	480
8	180	360	180	360
9	240	480	120	240
10	288	576	72	144

The experimental data being generated by finite element simulation, the contact area at maximum load was known and and first used in this method. However, this value is difficult to reach in practical situations, so comparison while using the area of the residual imprint instead of the real contact area, as well as result from the Oliver-Pharr method are provided. The maximum indentation depth used for the Oliver-Pharr method is 10 μm, so below 10% of the film thickness.

Table 6 Identified values

Material set	Identification method					
	Real contact area		Residual imprint		Oliver-Pharr	
	$E_f[GPa]$	Rel. error %	$E_1[GPa]$	Rel. error %	$E_1[GPa]$	Rel. error %
1	2.960	1.33	3.016	0.53	3.773	25.8
2	4.915	1.70	4.962	0.76	5.395	7.90
3	7.674	2.32	7.722	2.96	6.638	11.5
4	10.15	1.50	99.55	0.45	6.676	33.2
5	12.50	4.20	11.94	0.50	5.879	51.0
6	71.03	1.34	75.03	4.21	163.1	127
7	119.6	0.33	126.3	5.25	201.7	68.1
8	183.9	2.17	192.2	10.7	225.4	25.2
9	256.6	6.92	256.5	6.88	349.7	45.7
10	342.4	18.9	343.1	19.1	134.7	53.2

The results of the identification for the different methods are presented in Table 6. The identified values obtained from the residual imprint are slightly less precise than with the real contact area, this is more significant for the E/σ^Y ratio of $1/500$.

Apart from the material sets 5, 9, 10, the results are satisfactory. In these three cases related to harder films, the substrate deforms more, and some large rotations can be predicted for the film. The proposed method takes large displacement into account, but not the large rotations in the direct difference computation, therefore this is thought to be the cause of the discrepancy. These large rotations introducing geometrical non linearities could be dealt with, by extending the method with the use of the tangent stiffness matrix.

A better accuracy was reached than with Oliver-Pharr method. This can be explained mainly by the substrate and pile-up influence. The effect of the substrate is clearer on the material sets 1 to 5, a harder substrate leading overestimation of modulus while soft substrate to underestimation. For cases 6 to 9, this is balanced by the pile-up effect. As mentioned in the introduction, the Oliver-Pharr method relies on an estimation of the contact area which does not account for pile-up, the estimated value being smaler than the actual one, the Eq. (1) implying thus a overestimated Young modulus. However for the case 10, it can be supposed

that much of the deformations are carried by the substrate minimizing the pile-up effect, where the substrate effect predominates as for material sets 1 to 5.

7. Conclusions

A numerical method for identifying the Young's modulus of thin films by continuous indentation have been adressed. Its specificity is to compute the cost function gradient required in the inverse analysis, by a direct differentiation technique implemented directly in the finite element code, leading to a fast and precise way to obtain this gradient. Its validity was illustrated through comparison with finite difference and different numerical examples for the linear elastic case.

The method was addressed here in the restricted case of linear elastic materials, nevertheless its main interest is the possibility to be extended to materials with nonlinear behaviour (viscoelasticity, plasticity) by a similar approach, but by making use of the tangent stiffness matrix instead of the stiffness matrix.

Finally, by introducing a new cost function, a method for the evaluation of the Young's modulus of elasto-plastic thin films inverse analysis is suggested. Its main asset is to rely only on a an elastic model of the direct problem model in the inverse analysis, so that no assumption on the plastic behavior is needed, moreover the number of parameters to retrieve and computation time can be reduced, facilitating the identification. Its application on two numerical examples, for hard or soft coating, was discussed, showing its relevance.

Aknowledgements

J. Prou would like to gratefully acknowledge the Japanese Ministry of Education, Culture, Sports, Science and Technology for its support in his studies, and A. Constantinescu for the hospitality of the the Tokyo Institute of Technology during his stay as a visiting professor.

References

(1) D. Tabor, *Hardness of metals*. (1951) Clarendon, Oxford.
(2) A.C. Fischer-Cripps, *Introduction to Contact Mechanics*. (2000) Springer, Berlin.
(3) I. N. Sneddon, The relation between load and penetration in the axisymmetric boussinesq problem for a punch of arbitrary profile, *Int. J. Engng. Sci.*, 3 (1) (1965), pp. 47–57.
(4) K. Johnson, The correlation of indentation experiments, *J. Mech. Phys. Solids*, 18 (1970), pp. 949–956.
(5) L. Prandtl, *Proc. 1st Int. Cong. App. Mech.*, Delft, (1924), pp. 41–54.
(6) W. C. Oliver, G. M. Pharr, An improved technique for determining hardness and elastic modulus using load and displacement sensing indentation experiments, *J. Mater. Res.*, 7 (6) (1992), pp. 1564–1583.
(7) M. F. Doerner, W. D. Nix, A method for interpreting the data from depth-sensing indentation instruments, *J. Mater. Res.*, 1 (4) (1988), pp. 601–609.
(8) J. Loubet, J. Georges, O. Marchesini, G. Meille, Vicker's indentation curves of magnesium oxide (MgO), *J. Tribology*, 106 (1) (1984), pp. 43–48.
(9) G. Pharr, Measurement of mechanical properties by ultra low load indentation, *Mat. Sci. and Eng.: A* 253 (1998), pp. 151–159.
(10) J. He, S. Veprek, Finite element modeling of indentation into superhard coatings, *Surface and Coatings Technology*, 163-164 (30) (2003) pp. 374–379.
(11) F. Richter et al, Substrate influence in Young's modulus determination of thin films by indentation methods: Cubic boron nitride as an example, *Surface and Coatings Technology*, 201 (6) (2006), pp. 3577–3587.
(12) G. Bolzon, G. Maier, M. Panico, Material model calibration by indentation, imprint mapping and inverse analysis, *Int. J. Solids Struct.*, 41 (11-12) (2004), pp. 2957–2975.
(13) A. Constantinescu, N. Tardieu, On the identification of elastoviscoplastic constitutive laws from indentation tests, *Inverse Problems in Science and Eng.*, 9 (1) (2001), pp. 19–44.

(14) E. Tyulyukovskiy, N. Huber, Identification of viscoplastic material parameters from spherical indentation data: Part 1. Neural Networks, *J. Mater. Res.*, 21 (3) (2005), pp. 664–676.
(15) N. Tardieu, A. Constantinescu, On the determination of elastic coefficients from indentation experiments, *Inverse Problems* 16 (3) (2000), pp. 577–588.
(16) H. Li, J. J. Vlassak, Determining the elastic modulus and hardness of an ultra-thin film on a substrate using nanoindentation, *J. Mater. Res.*, 24 (3) (2009), pp. 664–676.
(17) Castem 2000 Finite Element Code webpage, available from http://www-cast3m.cea.fr/cast3m/index.jsp
(18) D. Tortorelli, P. Michaleris, Design sensitivity analysis: overview and review, *Inverse Problems in Engineering* 1 (1994), pp. 77–103.
(19) A. Srikanth, N. Zabaras, Shape optimization and preform design in metal forming processes, *Comp. Meth. Appl. Mech. Engng.* 190 (2000), pp. 1859–1901.
(20) S. Stupkiewicz, J. Korelc, M. Dutko, T. Rodic, Shape sensitivity analysis of large deformation frictional contact problems, *Comp. Meth. Appl. Mech. Engng.* 191 (33) (2002), pp. 3555–3581.